Precision Agriculture
https://doi.org/10.1007/s11119-020-09768-6

Normalization of the crop water stress index to assess the within-field spatial variability of water stress sensitivity

Victoria Gonzalez-Dugo[1] · Pablo J. Zarco-Tejada[1,2] · Diego S. Intrigliolo[3] · Juan-Miguel Ramírez-Cuesta[3]

Accepted: 20 October 2020

Abstract

This paper presents a novel methodology for identifying homogeneous areas within high-frequency drip-irrigated orchards and for defining the most sensitive and resistant areas of the field to water stress. The methodology proposed here is based on the assessment of water status at the tree level during mild water stress using remote sensing derived indicators which provide valuable information about the spatial distribution of the response to water stress within an orchard. The areas more resistant to water stress will maintain a good water status, while those prone to water stress will develop initial symptoms of water deficit. The study was performed over three different peach orchards that were evaluated from 2 to 3 years. Water status was monitored using high-resolution thermal imagery acquired before and after the onset of water stress. The Thermal Sensitivity Index (TSI), derived from the difference of the CWSI and the cumulated reference evapotranspiration between the two dates, demonstrated to be well related to the increase of stem water potential. The spatial distribution of TSI enables the identification of sensitive areas within a peach orchard, a first step for establishing precision drip irrigation programs.

Keywords CWSI · High-resolution remote sensing · Thermal · Management zone · Sensitive areas · Peach orchard

✉ Victoria Gonzalez-Dugo
victoria.gonzalez@ias.csic.es

[1] Instituto de Agricultura Sostenible (IAS), Consejo Superior de Investigaciones Científicas (CSIC), Alameda del Obispo s/n, 14004 Cordoba, Spain

[2] Department of Infrastructure Engineering, Faculty of Veterinary and Agricultural Sciences (FVAS), School of Agriculture and Food, Melbourne School of Engineering (MSE), University of Melbourne, Melbourne, VIC 3010, Australia

[3] Dpto. Riego, Centro de Edafología y Biología Aplicada del Segura (CEBAS-CSIC), P.O. Box 164, 30100 Murcia, Spain

Introduction

Agricultural fields are naturally heterogeneous and this variability is often related to soil properties, mainly variations in slope, texture, depth and mineral composition (Camp and Sadler 1998). These factors are static or relatively stable from year to year, and have been used in the past to delineate management zones, or at least, to identify homogeneous areas within fields (Schepers et al. 2004; Bazzi et al. 2019). The identification of these management units is particularly relevant for the optimized use of external inputs and for irrigation purposes. Considering the current situation of water availability and future climate change scenarios, it is essential to identify strategies to save water while maintaining crop productivity by the efficient use of water through improved management and advanced irrigation technologies. Deficit irrigation strategies, irrigation technologies to reduce the leaching and water losses, and precision irrigation are examples of the available techniques that can be implemented to increase water use efficiency.

A preliminary understanding of the field heterogeneity is essential for applying these strategies. This assessment is critical for the definition of management zones, defined as sub-areas with a relative homogeneity in crop production potential, due to similar soil nutrients and environmental effects caused by similar landscape or soil conditions (Yan et al. 2007). Therefore, this concept is strongly connected to soil properties. Focusing on soil properties to delineate homogeneous areas in the field is challenging. Physical properties such as slope and orientation are now relatively easy to monitor by the use of digital elevation models (DEM). However, monitoring some other properties, such as soil depth and mineral composition, is labor- and time-consuming. Additionally, there are other sources of variability that increase the differences in crop output and/or yield. Some of these factors are dynamic and may change along the crop cycle, such as water and nutrients availability or crop health (Hsiao et al. 1976). The complexity of monitoring field variability from soil properties can be overcome by developing a methodology based on crop performance. Crop growth and development is affected by soil texture, chemical properties, as well as nutrient and water availability. Therefore, the development of a plant-based methodology would provide an easy and accurate approach for characterizing the overall effect of field heterogeneity on crop performance, which is the final objective of agricultural practices.

The identification of those areas most sensitive to water stress within a field might be of special interest for several reasons, such as the optimization of the irrigation system design (Gonzalez-Dugo et al. 2015) and the selection of optimum field locations for the installation of soil and plant sensors (Bazzi et al. 2019). Based on the strategic decision adopted by the grower according to economic and agronomical aspects, sensors might be installed in average areas (that will provide information of the mean crop water status in the field), or it can be installed in those areas that are most sensitive to water stress (that will provide an early warning about water shortage).

Finally, this information can be helpful in precision irrigation strategies, where the grower has the ability to irrigate the field according to local water requirements. Variable rate irrigation (VRI) systems, such as pivots or lateral move irrigation machines, provide such flexibility of delivering water in a variable rate, according to local demand. These systems require detailed information about crop water needs in order to optimize its use. The combination of management zone maps and VRI systems has been demonstrated to be very effective at delivering site-specific water application (Dukes and Perry 2006; O'Shaughnessy et al. 2015).

Remote sensing (RS) methods appear as a suitable alternative to the use of ground-sensors for identifying homogeneous zones. High-resolution RS enables the assessment of water status and crop performance over large areas, with sufficient resolution to identify individual trees in the field. The close relationship between canopy transpiration and surface temperature allows using thermal imagery to derive crop water status (Jones et al. 2002; Ben-Gal et al. 2009; Ramírez-Cuesta et al. 2017), to monitor irrigation requirements (Bellvert et al. 2016) and to identify areas sensitive to water stress under low-frequency irrigation systems (Gonzalez-Dugo et al. 2015). In order to use canopy temperature as a water status indicator, it has to be normalized to account for the environmental conditions (Agam et al. 2013; Conesa et al. 2019). The normalization is often carried out by the development of indices, such as the Crop Water Stress Index (CWSI; Idso et al. 1981), which is the most commonly used indicator derived from canopy temperature.

Previous studies have used plant-derived information to delineate management zones. McClymont et al. (2012) developed a methodology for delineating homogeneous subzones in vineyards based on the assessment of NDVI and canopy temperature at a specific time. Cohen et al. (2017) highlighted the need for a dynamic definition of irrigation management zones based on thermal images by showing the in-season spatial changes in water status. Promising results have been obtained also in variable rate irrigation systems by using dynamic prescription maps derived from thermal information (O'Shaughnessy et al., 2015). These maps provided valuable information for scheduling irrigation with no losses in crop yield when compared to soil moisture-based irrigation scheduling methods. In orchard trees, such a dynamic approach over large areas requires multiple high-resolution aerial imagery acquisitions, which can be expensive and labor-consuming. On the other hand, the static approach depends on the instantaneous water status and may not capture all the variability of water status as water stress is imposed. Additionally, a static CWSI has some drawbacks that require special attention such as the definition of upper and lower baselines for a proper CWSI calculation. These thresholds can be dependent on the crop variety, the crop load, and the leaf age, among other factors (Gonzalez-Dugo et al. 2014). Thus, it would be desirable to develop a methodology to capture dynamic variations of water status while minimizing the requirements of aerial acquisitions and the specifications of the indicator used to monitor water stress. Gonzalez-Dugo et al. (2015) developed a CWSI-based methodology that enables the identification of the most sensitive areas to water stress within a pistachio orchard under low-frequency irrigation. Nevertheless, such a methodology cannot be used under a high-frequency irrigation scheme, as it is based on normalizing CWSI with the number of days since last irrigation. Depending on the soil properties and soil water reserves, water stress in drip irrigated fields would appear at a very slow rate, making the use of such a method unreliable. Therefore, such methodology needs to be adapted to daily irrigated fields.

The objective of this work is to develop a RS-based methodology derived from thermal imagery for identifying homogeneous areas within agricultural fields and for defining the most sensitive and resistant areas to water stress. The identification of such areas is of special interest when a limited number of sensors are planned to be deployed in the field as well as for precision irrigation purposes.

Materials and methods

The methodology proposed with the aim of identifying the sensitive area prone to water stress consisted of developing a mild water stress throughout the orchard, based on the rate of change of water status between two dates, before and after a period of irrigation withholding. The main hypothesis is that the areas more resistant to water stress will maintain a good water status, while those prone to water stress will develop initial symptoms of water deficiency at an earlier stage. To compute this, the entire orchard must be under well-watered conditions at the beginning of the experiment, and for a short period, irrigation must be withheld, in order to develop the required mild water stress condition.

Study site description

The experiment was performed in three study sites: (i) a peach orchard (*Prunus persica* var. Amandine) of 3.4 ha planted in 2013 (hereafter Amandine; Fig. 1); (ii) a peach orchard (*Prunus persica* var. Nazario and *Prunus persica* var. Plawhite5) of 6.4 ha planted in 2005 (Plawhite5) and 2009 (Nazario) (hereafter Nazario; Fig. 1); and (iii) a flat peach orchard (*Prunus persica* var. Carioca) of 6.7 ha planted in 2010 (hereafter Carioca; Fig. 1). All sites

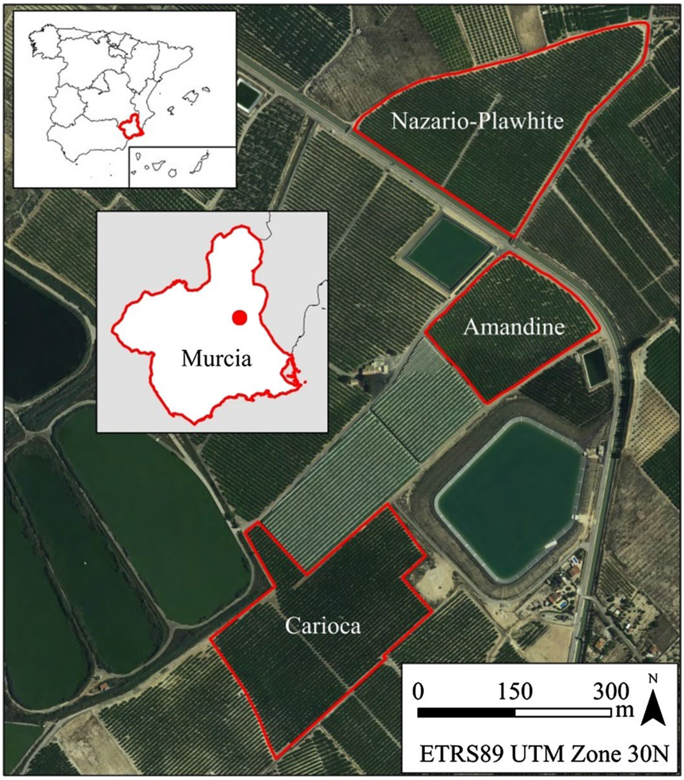

Fig. 1 Aerial image and location of the three experimental sites used in the study. The area of study is located in southern Spain in the region of Murcia (38°06′N, 1°12′W)

are drip irrigated with two irrigation lines resulting in a total density of 12 drippers of 1.6 l h^{-1} per tree. The row and plant spacing for the three sites were 5 and 3.5 m, respectively.

Fields were subjected to cycles of mild water stress, three cycles for Amandine field (2016–2018) and two for Carioca and Nazario (2017–2018). These cycles consisted on maintaining the trees in a good water status, inducing water stress by the lack of irrigation during a period of several days (from 3 to 6 days; Table 1). These cycles were applied at the post-harvest period, which is considered as a period less sensitive to water shortage. Indeed, it is suggested as a suitable phase to apply regulated deficit irrigation in early-maturing cultivars, such as those selected for this study (Johnson et al. 1992; Girona and Fereres 2012).

Field measurements

Prior to the application of the cycles of mild water stress, irrigation uniformity was measured in order to ensure that the obtained results were not influenced by large differences in dripper water application.

Additionally, stem water potential (Ψ_s) was measured when trees were well-irrigated (Date 1 in Table 1) and after inducing water stress (Date 2). Ψ_s was measured at midday by means of a pressure chamber (Model 600, PMS Instrument Company, Albany, OR, USA) on west side-oriented and non-transpiring leaves previously bagged in hermetic plastic bags covered with aluminum foil for at least 1 hour before measurements. The number of Ψ_s measurements is indicated in Table 1.

Airborne imagery

In order to analyze the spatial variability of water status throughout the orchard, two aerial observations per year were conducted. The airborne operations were carried out on July-August of 2016–2018 (Table 1), corresponding with Date 1 and Date 2 (Table 1).

Flights were performed on the solar plane (i.e., with the sun on the tail plane) to avoid solar bi-directional effects across the image, using a thermal camera and a micro-hyperspectral imager installed in tandem on a Cessna aircraft operated by the Laboratory for Research Methods in Quantitative Remote Sensing (QuantaLab), Consejo Superior de Investigaciones Científicas (IAS-CSIC, Spain). The thermal imagery was acquired in the 7.5–13 µm range with the FLIR SC655 thermal camera (FLIR Systems, Wilsonville, OR, USA). The camera yields a resolution of 640×480 pixels equipped

Table 1 Summary of the study sites, the start and end of the irrigation withholding period and the number of stem water potential (Ψ_s) measurements performed

Site	Year	Date 1	Date 2	N (Ψ_s)[a]
Amandine	2016	1 August	4 August	245
	2017	18 July	24 July	78
	2018	2 July	6 July	75
Carioca	2017	18 July	24 July	175
	2018	2 July	6 July	75
Nazario	2017	18 July	24 July	147
	2018	2 July	6 July	75

[a]The indicated number corresponds to the measurements performed at each date

with a 13.1 mm optical focal length, providing an angular FOV of 45° and a ground resolution of 25 cm when flying at 200 m above ground level (AGL). The camera's radiometric calibration was assessed in the laboratory using a blackbody (model P80P, Land Instruments, Dronfield, United Kingdom). After each flight, thermal images were processed in the laboratory and mosaicked to generate the entire scene of surface temperature. The linear-array hyperspectral camera used in this study was the micro-hyperspec VNIR model (Headwall Photonics, Fitchburg, MA, USA) operated with a configuration of 260 spectral bands acquired at 1.85 nm pixel-1 and 12-bit radiometric resolution in the 400–885 nm region, yielding a 6.4 nm FWHM with a 25-micron slit and 20 cm resolution at the indicated flight altitude. For more information about camera settings and configuration, see Zarco-Tejada et al. (2012). The micro-hyperspectral sensor was radiometrically calibrated in the laboratory using an integrating sphere (LabSphere, North Sutton, NH, USA) at four levels of illumination and six integration times. The integrating sphere is an optical component consisting of a hollow spherical cavity with its interior covered with a diffuse white reflective coating, with small holes for entrance and exit ports providing calibrated radiance levels.

Image processing

Once the imagery was mosaicked, regions of interest were determined to identify pure vegetation pixels and to extract the canopy temperature and reflectance from each individual tree crown, as was described in Gonzalez-Dugo et al. (2019). Trees were identified using a fishnet methodology that created a mesh that was applied in all flights to get the same ID for each tree. Finally, CWSI and NDVI for the individual trees were computed for each date from thermal and hyperspectral data, respectively.

The mean value for each tree was used to calculate spectral indices (as described in "Crop water status assessment" section and "Development of the index" section). These values were interpolated by kriging to derive the maps using the software ArcMap® (v10.5; Esri, Redlands, CA, USA).

Crop water status assessment

The CWSI was used to assess the crop water status and its temporal evolution, which is computed using the following equation:

$$CWSI = \frac{\left(T_c - T_a\right) - \left(T_c - T_a\right)_{LL}}{\left(T_c - T_a\right)_{UL} - \left(T_c - T_a\right)_{LL}} \tag{1}$$

where $T_c - T_a$ is the temperature difference between the canopy (T_c) and the air (T_a); and the subscripts LL and UL indicate the lower and upper limits, corresponding with non-water stressed trees and non-transpiring trees, respectively. The lower limit was determined according to the non-water stress baseline (NWSB) developed by Berni et al. (2009). The upper limit was calculated using the methodology proposed by Idso et al. (1981) and corresponds with the intercept of the NWSB modified by the difference in vapor pressure induced by the $T_c - T_a$ value. This index varies from 0 for non-stressed crops, to 1 for severely affected trees.

Development of the index

The new index developed here allows computing the increase of water stress after a mild water shortage. This index will serve as a basis to assess the sensitivity of any given area of the field to water stress, based on the increase of the CWSI for each tree from Date 1 to Date 2 ($CWSI_2 - CWSI_1$). But other aspects affecting the increase of CWSI between the two dates must also be taken into account. Under theoretical well-watered conditions, the CWSI on day 1 is expected to be equal to 0 throughout the orchard. But the natural variability that usually occurs in the field often results in a gradient of CWSI. For this reason, the term ($1 - CWSI_1$) is proposed to be included into the definition of the index.

The climatic conditions occurring between the two dates must also be considered, as the rate of increase of CWSI will depend on the evaporative demand during the water shortage period. The cumulated reference evapotranspiration (ΣET_o) was used to compute the environmental conditions during the experiments. The climatic data were obtained from a meteorological station from the SIAM network (http://siam.imida.es), located at 1 km distance from the study area.

Taking these issues into account, the final formulation for the proposed index is as follows (Eq. 2):

$$TSI = \frac{(CWSI_2 - CWSI_1)}{\left(1 - CWSI_1\right) \cdot \sum_{t=1}^{2} ETo} \tag{2}$$

This index has been named as Thermal Sensitivity Index (TSI; mm^{-1}), being subscripts 1 and 2 the values for the first and second day of data acquisition, respectively.

Statistical analysis

The CWSI–Ψ_s data were randomly split into two parts, containing 75% of the observations (training dataset) and the remaining 25% as the testing dataset. The training dataset was used to build the models relating the CWSI-based formulations and the rate of change of water potential, while the independent testing dataset was used to test the models. The model performance was evaluated using the root mean square error (RMSE), the relative root mean square error (RMSEr), the mean absolute error (MAE) and the mean absolute percentage error (MAPE).

Clusters of high and low values (hot spots) detected in the maps derived from the TSI were identified using the Getis-Ord Gi* statistics in ArcMap 10.1 (spatial statistic tools). This tool evaluates each feature within the context of neighboring features. A feature with a high value is interesting but may not be a statistically significant hot spot. To be a statistically significant hot spot, a feature will need to have a high value but also be surrounded by other features with high values as well. This tool was used to identify such areas sensitive and resistant to water stress.

Results

Plant water status

Stem water potential

Figure 2 shows the average values of Ψ_s measured in all study sites for both well-irrigated and water-stressed conditions (Date 1 and Date 2 in Fig. 2, respectively). Initial Ψ_s values (Date 1) were close to − 10 bar for all study sites in the different campaigns; although the higher Ψ_s values measured in 2018 in all varieties suggest that in this crop season the trees were closer to the optimum water conditions than in 2017. The Ψ_s associated with the water stress cycle decreased to values ranging between −15 and −21 bar, the last observed in Amandine 2016. Comparing the effects on the different varieties, Amandine experienced the highest Ψ_s decrease between the two dates ($|\Psi_{s,2} - \Psi_{s,1}|$; $\Delta\Psi_s$ ranged from 7.6 to 9.8 bar) whereas Carioca and Nazario showed lower Ψ_s reductions ($\Delta\Psi_s$ ranged from 4.9 to 5.5 bar).

Crop water stress index

The CWSI maps demonstrated large variability of crop water status on the two measurement dates (Figs. 3, 4 and 5). In all study sites, CWSI in Date 1 ($CWSI_1$) was consistently lower than CWSI in Date 2 ($CWSI_2$). In Amandine site, average $CWSI_1$ ranged from 0.03 to 0.15 whereas average $CWSI_2$ reached values of 0.53 (Table 2; Fig. 3). $CWSI_1$ estimates in Carioca and Nazario sites resulted greater than Amandine, with values of 0.24–0.35, whereas $CWSI_2$ was similar than in Amandine site, with values ranging from 0.42 to 0.50 (Table 2; Figs. 3 and 5). Additionally, the variability observed in CWSI was slightly higher in Date 2 than in Date 1, as reflected in the standard deviation values (Table 2; Figs. 3, 4 and 5). When observing the variation of CWSI between both dates ($CWSI_2$-$CWSI_1$; ΔCWSI), it can be observed that each field responded differently to the same water stress level. In Amandine site, the ΔCWSI ranged from 0.27 (2018) to 0.42 (2016) (Table 2;

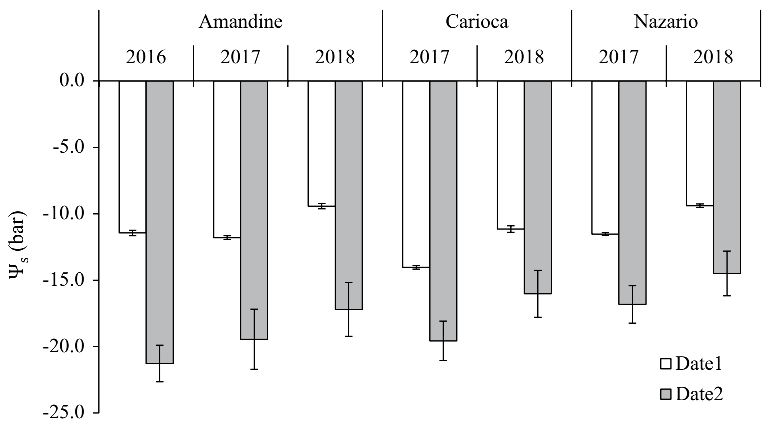

Fig. 2 Average values of stem water potential (Ψ_s) for the different crop seasons

Table 2 Average values and standard deviations of $CWSI_1$ and $CWSI_2$ for all study sites

Crop season	Parameter	Mean	St. Dev
Amandine 2016	$CWSI_1$	0.03	0.11
	$CWSI_2$	0.46	0.15
	ΔCWSI	0.42	0.11
Amandine 2017	$CWSI_1$	0.15	0.13
	$CWSI_2$	0.53	0.14
	ΔCWSI	0.35	0.11
Amandine 2018	$CWSI_1$	0.15	0.09
	$CWSI_2$	0.41	0.16
	ΔCWSI	0.27	0.10
Carioca 2017	$CWSI_1$	0.35	0.12
	$CWSI_2$	0.50	0.14
	ΔCWSI	0.14	0.09
Carioca 2018	$CWSI_1$	0.24	0.06
	$CWSI_2$	0.39	0.10
	ΔCWSI	0.15	0.08
Nazario 2017	$CWSI_1$	0.27	0.10
	$CWSI_2$	0.45	0.12
	ΔCWSI	0.18	0.11
Nazario 2018	$CWSI_1$	0.24	0.08
	$CWSI_2$	0.42	0.12
	ΔCWSI	0.20	0.11

Fig. 3); whereas Carioca and Nazario displayed a ΔCWSI lower than 0.20 (Table 2; Figs. 4 and 5).

Stem water potential–crop water stress index relationship

The relationship between Ψ_s and CWSI at the time of flight was significant and displayed a similar regression line for the three experimental sites and years, yielding $R^2 = 0.59$ (Fig. 6). For CWSI values below 0.2, Ψ_s was maintained rather stable and close to − 10 bar. Beyond this threshold of CWSI, the Ψ_s sharply decreased. The maximum value of CWSI observed in the monitored trees was 0.77, corresponding with a value of Ψ_s close to − 25 bar (Fig. 6).

Thermal Sensitivity Index

The first step was to develop an indicator related to the rate of change of Ψ_s ($\Delta\Psi_s/n$, MPa day^{-1}) in monitored trees, calculated as the difference between the two readings, divided by the number of days elapsed between them ($\Delta\Psi_s/n$). The simplest formulation tested was the difference between the CWSI values of the two dates ($CWSI_2$–$CWSI_1$, ΔCWSI). Results yielded a low correlation when related to $\Delta\Psi_s/n$, with increased dispersion of data, especially as the level of water stress raised (Fig. 7a). When the formulation took into account the term ($1 - CWSI_1$), the overall R^2 decreased (Fig. 7b) but the regressions slightly improved for the individual datasets (R^2 ranged between 0.01 and 0.33 in

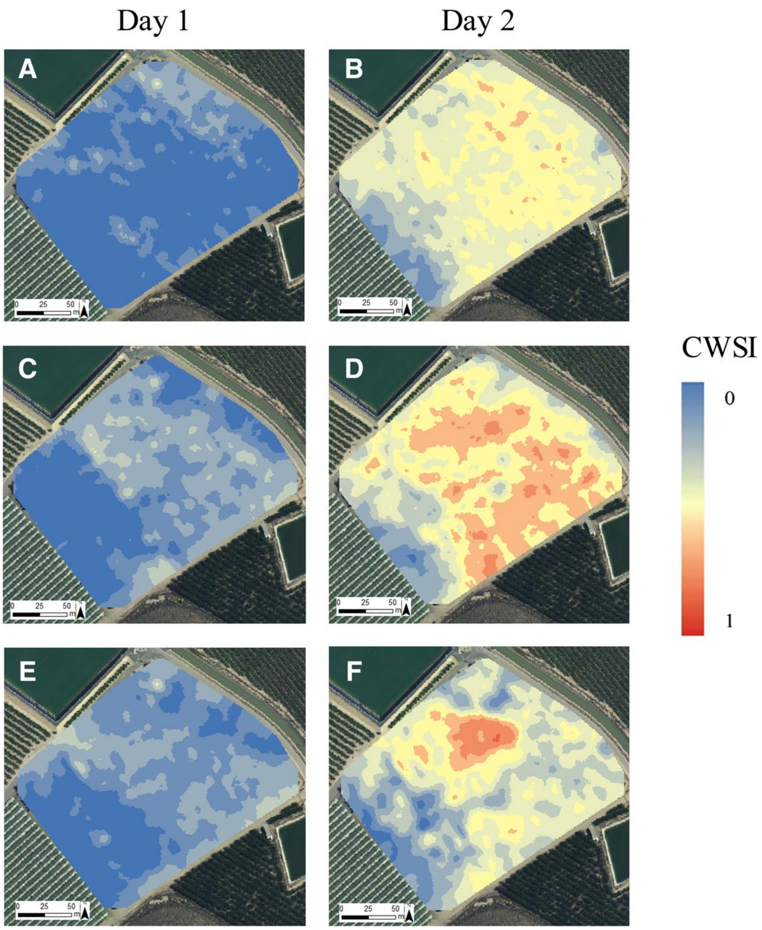

Fig. 3 Interpolated maps of CWSI of Amandine site in 2016 (**a** and **b**), 2017 (**c** and **d**) and 2018 (**e** and **f**). Left column corresponds with the first flight, before irrigation cutoff, and right column corresponds with the second flight

Fig. 7a and from 0.11 to 0.48 in Fig. 7b). There were clear differences among the regressions for the study sites. When the increase of CWSI was normalized by the cumulated ET_o, the overall regression improved significantly ($R^2 = 0.56$) (Fig. 7c). Finally, when the formulation was computed according to Eq. 2, the regression obtained the best adjustment, with an R^2 equal to 0. 59. The index was also tested by including the NDVI in the denominator, but the performance was similar to the actual formulation (*data not shown*). The test data set was used to analyze the performance for the four models included in Fig. 7 (Table 3). The lowest values of RMSE and the relative RMSEr were observed in the TSI (0.68 and 39%, respectively). MAE and MAPE of TSI displayed similar values than $\Delta CWSI/\Sigma ET_o$ (0.52 and 46%, respectively), and clearly lower than the other two formulations, with MAE ranging from 0.52 to 0.59 and MAPE varying from 0.64 to 0.69.

Once the index was formulated and compared to the ground truth data, it was applied to the entire imagery to estimate the $\Delta\Psi_s/n$ and analyze its spatial variability (Fig. 8). There were some variations between the years, although some similarities were also observed.

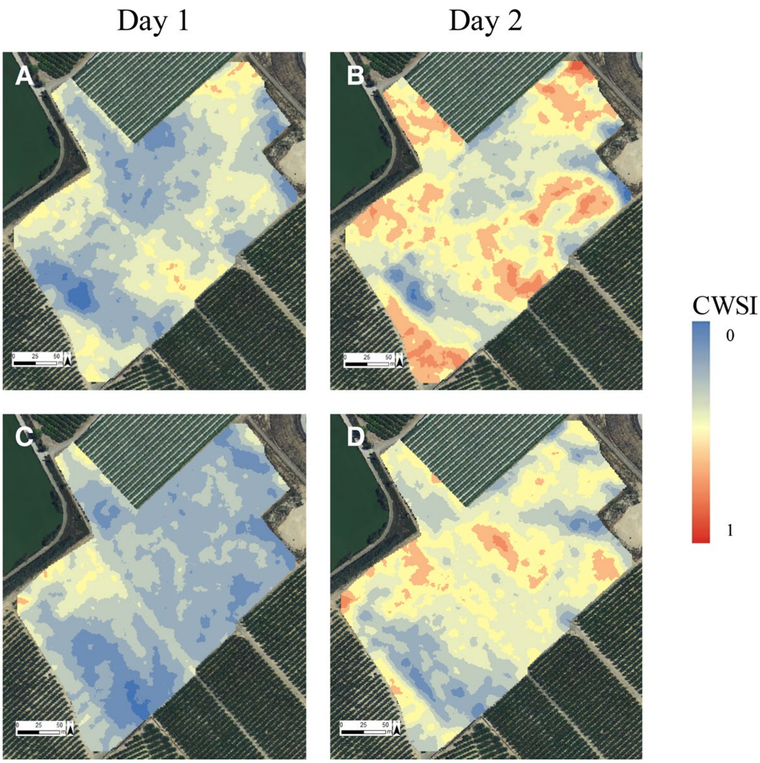

Fig. 4 Maps of CWSI of Carioca site in 2017 (**a** and **b**) and 2018 (**c** and **d**). Left column corresponds with the first flight, before irrigation cutoff, and right column corresponds with the second flight

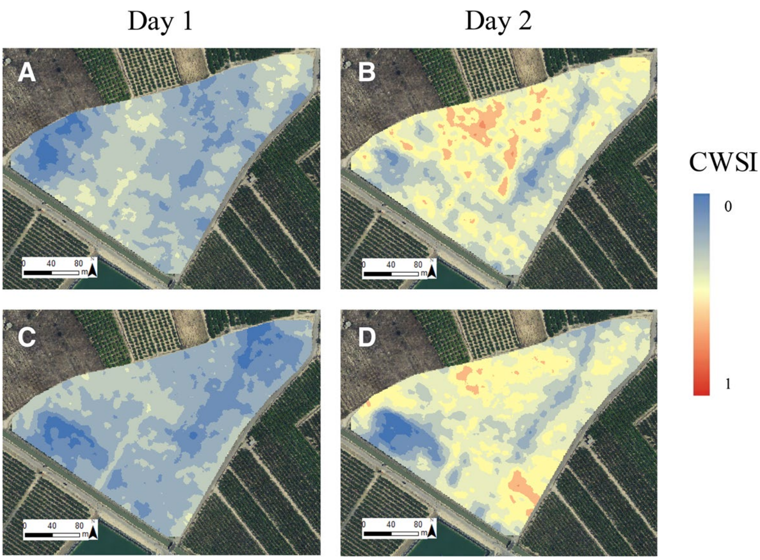

Fig. 5 Maps of CWSI of Nazario site in 2017 (**a** and **b**) and 2018 (**c** and **d**). Left column corresponds with the first flight, before irrigation cutoff, and right column corresponds with the second flight

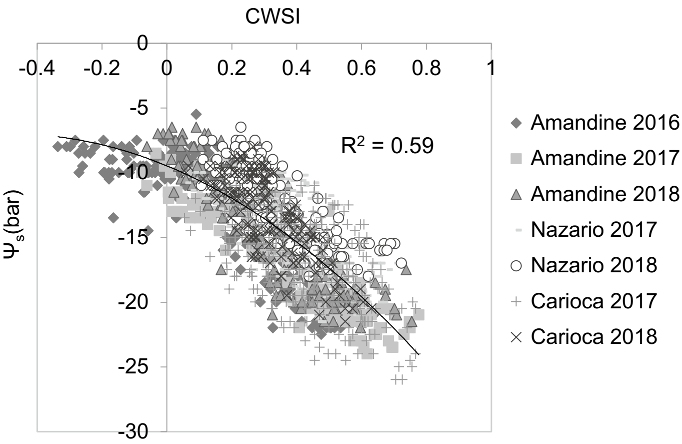

Fig. 6 Relationship between CWSI and Ψ_s for the complete dataset (N = 1 509). The regression was adjusted to the seven datasets

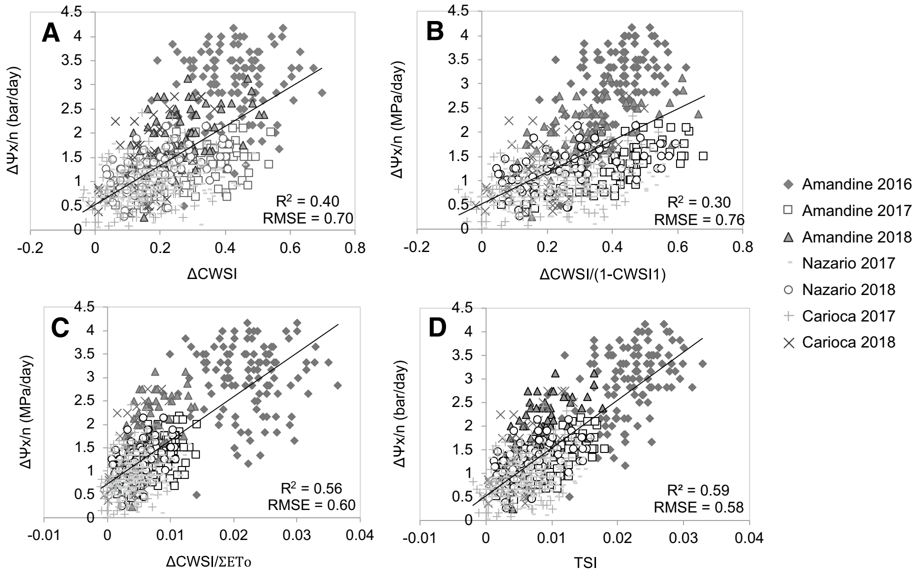

Fig. 7 Relationship between the rate of change of the Ψ_s ($\Delta\Psi_s/n$, bar day^{-1}) between the two dates and the difference between the two CWSI values (ΔCWSI, **a**), the difference between the two values of CWSI normalized by the initial value of CWSI ($\Delta CWSI/(1 - CWSI_1$; **b**), the difference between the two values of CWSI normalized by the cumulated thermal time ($\Delta CWSI/\Sigma ET_o$, **c**) and the Thermal Sensitivity Index, as defined in Eq. 2 (TSI, **d**). The number of observations for the training dataset was 537

This type of spatial analysis enables the identification of areas with a similar sensitivity to water shortage. In Fig. 9, the hot spots areas were identified according to the Gi* statistics.

According to the analysis based on the Gi* statistics, the percentage of the total area that was similarly classified across years ranged between 45 and 65%. The area that was identified as hot spot in all the crop seasons over the fields can be observed in Fig. 10.

Table 3 Root mean square error (RMSE; bar day^{-1}), relative RMSE (RMSEr), mean absolute error (MAE; bar day^{-1}) and mean absolute percentage error (MAPE) calculated for the models considered in the study using the test data set

	RMSE	RMSEr (%)	MAE	MAPE (%)
$\Delta\Psi_s/n = f(\Delta CWSI)$	0.72	49	0.52	64
$\Delta\Psi_s/n = f(\Delta CWSI;\ 1 - CWSI1)$	0.79	53	0.59	69
$\Delta\Psi_s/n = f(\Delta CWSI;\ \Sigma ET_o)$	0.61	41	0.42	56
$\Delta\Psi_s/n = f(TSI)$	0.68	39	0.42	56

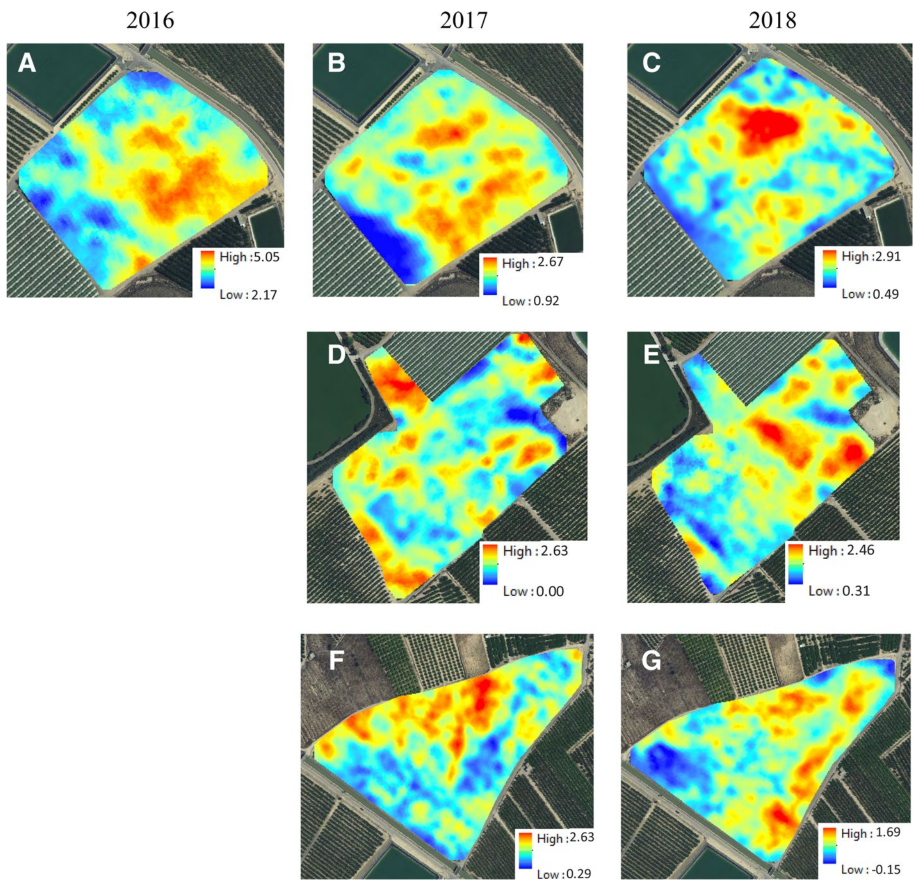

Fig. 8 Spatial pattern of the $\Delta\Psi_s/n$ obtained from TSI values in Amandine site (**a** to **c**), Carioca site (**d** and **e**) and in Nazario site (**f** and **g**), in 2016 (**a**), 2017 (**b**, **d** and **f**) and 2018 (**c**, **e** and **g**)

Discussion

This study presents a methodology to assess the sensitivity to water stress in orchard fields under high-frequency drip irrigation. The management zones are usually established according to stable soil properties (Yan et al. 2007). This approach, although effective,

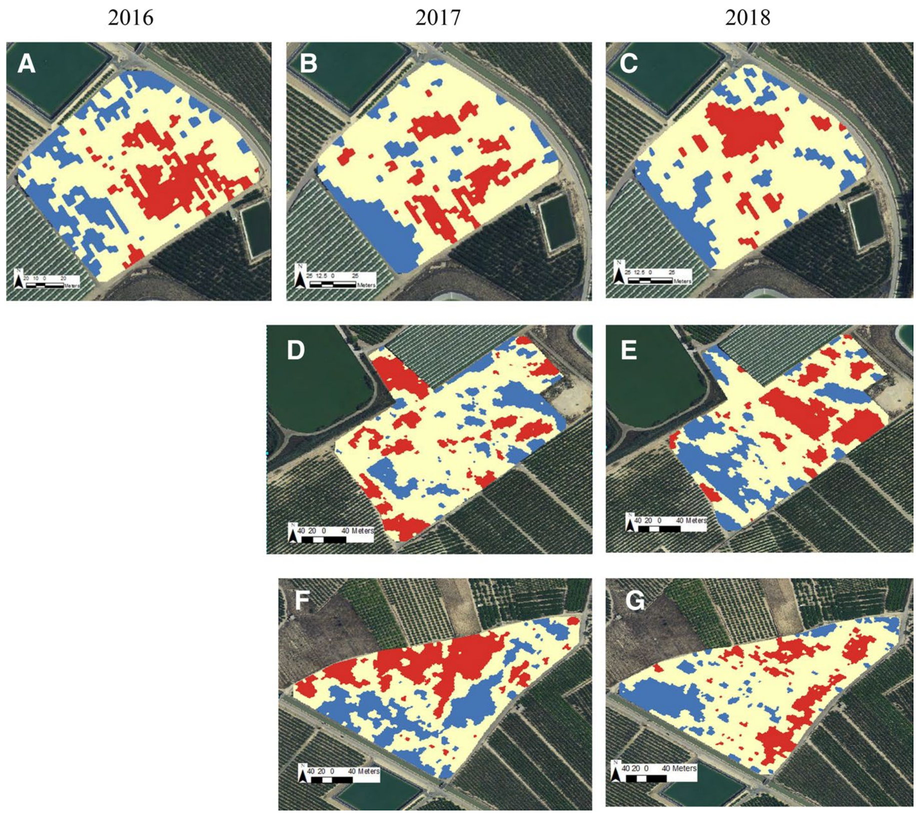

Fig. 9 Identification of hot spot areas that demonstrated the highest (red) and lowest (blue) sensitivity to water stress, according to TSI in Amandine site (**a** to **c**), Carioca site (**d** and **e**) and in Nazario site (**f** and **g**), in 2016 (**a**), 2017 (**b**, **d** and **f**) and 2018 (**c**, **e** and **g**), based on the Gi* statistic (Color figure online)

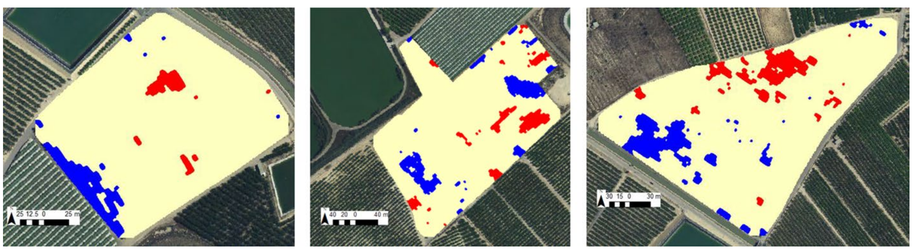

Fig. 10 Areas identified as hot spot in all the crop seasons over the study sites. Blue color corresponds to areas resistant to water stress, while red indicates sensitive areas (Color figure online)

requires a substantial effort acquiring soil samples for properly characterizing soil chemical and physical characteristics. The development of a methodology exclusively based on the crop response to water availability, derived from RS imagery, avoids such limitation. This strategy enables the assessment of the final effect of both static (e.g. soil texture, nutrient status) and dynamic factors (e.g. weather conditions, crop management) over the crop growth and development. The methodology presented here is based on the assessment of the Thermal Sensitivity Index (TSI), which is derived from the information obtained from the CWSI acquired at two different dates and the evaporative demand accumulated between the two measurements. The TSI was consistently related to the rate of change of Ψ_s for the range of sensitivity to water stress observed in this study (from 0 to 4 bar day^{-1}). It was demonstrated that the TSI developed here performs better than the rest of the formulations tested. In addition to yielding higher R^2 values compared to the others ($R^2=0.58$ vs. $R^2=0.30$–0.56), the measures calculated in the analysis of the model performance presented in Table 3 displayed the lowest error values. Moreover, the difference between the RMSE and MAE was minimal for the TSI-based model, indicating the smallest variance in the individual error of the sample and a more distributed dispersion of the error in the whole range.

In comparison with a single assessment of CWSI, this methodology enables the analysis of the rate of change of water status during a given period, taking into consideration the initial and final conditions, and the evaporative demand (in terms of ET_o) between the two dates.

The increase in variability of the CWSI for the second date compared to initial values before the onset of water stress (as it was observed in the standard deviation values, Table 2) indicates that trees respond differently to water stress. This intra-orchard variability can be related to differences in soil properties, available water content, crop management, and crop health, among other factors. Tree size might also influence significantly the variation of CWSI between the two dates. On one hand, large trees will deplete soil water content more rapidly, so it is expected to increase the sensitivity to water stress. On the other hand, large trees could have more developed root systems, enabling them to access a larger volume of available water. In this study, including NDVI in the formulation did not improve the assessment of the sensitivity to water stress. This is probably related to the small range of variation of NDVI observed in the three fields, but also due to the relatively high NDVI values observed (0.8 ± 0.07). It is well known that NDVI is not sensitive to difference in tree vigor under relatively dense canopy conditions (LAI > 3; Gilabert et al. 1996). Further research regarding the effect of contrasted tree size and on the use of other vegetation indices less affected by saturation (e.g. based on red-edge spectral region and based on normalized ratios) may be of interest for widening the use of this methodology.

It is well-accepted that thermal imagery is one of the most suitable methods to retrieve water status over large areas (Jones et al. 2002). Nevertheless, it is important to identify the constraints of this methodology. High resolution thermal imagery requires specific airborne flights, which might have a relatively high cost, especially compared to satellite imagery freely available. Moreover, thermal imagery should be acquired around midday on cloudless days in order to reliably retrieve water status as it has been observed previously (Testi et al. 2008). This can limit the total area that can be monitored. Although in this study promising results using a large dataset (comprising three areas and 2 to 3 years) have been obtained, it would be desirable to assess TSI robustness over different crops as well as climates.

The patterns of the ΔCWSI observed for the three fields were different. Nazario and Carioca displayed a lower ΔCWSI compared to Amandine for both years 2017 and 2018 (Table 1). It was related to a higher CWSI on Date 1, and a smoother development of water stress. In Amandine plot, although initial CWSI was relatively lower than that of the other two fields, the rate of increase of CWSI was higher. It can be hypothesized that soil water reserves in Amandine field were lower than those of the two other experimental sites, resulting in a sharp increase of CWSI during the experiment, even if the initial water status was more favorable. Moreover, some studies have reported a contrasted sensitivity of different peach cultivars to water stress (Girona and Fereres 2012). Further studies assessing the sensitivity of the cultivars used to water stress would provide more information about the contribution of this effect to the results observed here.

The study performed in August 2016 in Amandine displayed the highest values of $\Delta\Psi_s$ and ΔCWSI. In water scarce situations, the irrigation is scheduled to optimize soil water use, depleting progressively the water reserves as the season advances. As a consequence, an irrigation withholding later in the season might reveal a higher sensitivity (for the same evaporative demand). It is in accordance with the dynamic variation of the maps resulting from this methodology, which partially vary from year to year. Although the index is a step forward as it considers the rate of change of CWSI and the evaporative demand during the time of the measurements, there are factors, such as the depletion of soil water reserves, which are not captured by the current formulation. This is the reason why absolute values were different among the different campaigns, and the index must be analyzed in relative terms. The use of the methodology and the index developed in this study has to consider this aspect. The application of this system at the beginning of the irrigation season might decrease the effect of those factors and provide with information about the crop water status. Replicating the system several times during the irrigation season might increase understanding about the pattern of water status throughout the cycle.

The identification of homogeneous areas can be useful for the proper development of several strategies aiming at improving water productivity. It can help decision making when deficit irrigation is sought to be applied, as the level of water stress developed in sensitive areas may be detrimental for tree performance (Fereres and Soriano 2007). By combining the information provided by the TSI with the crop production function (that relates the crop yield and the water used), it is possible to implement models to assess the decline in production resulting from different irrigation strategies. Particularly under regulated deficit irrigation, it is crucial to avoid mild water stress that becomes too severe and detrimental for tree performance (Fereres and Soriano 2007). The data resulting from this study showed that under standard irrigation practices there is large variability in water status. If deficit irrigation strategies are applied under these circumstances, particularly in stone fruit trees, crop yield might be severely affected under some areas (Fereres et al. 2003).

In addition to this, the reasons for developing methods aiming at identifying sensitive areas within fields are multiple: identification of failures in irrigation systems design, identification of areas to install point sensors, and precision irrigation. Gonzalez-Dugo et al. (2015) developed a methodology to identify sensitive areas to water stress for fields irrigated at low frequency. Dag et al. (2015) developed a methodology to automatically detect irrigation malfunctions, based on the analysis of the temperature histogram of the field. The procedure presented here analyzes the rate of increase of the CWSI over a certain period of time, so initial conditions are also considered. When trees are irrigated at daily scale, patterns of water stress are not easily observed, because trees are normally continuously well-irrigated. When deficit irrigation is applied and the water stress is generalized to the entire orchard, sensitive areas cannot be distinguished either. It is necessary to analyze crop performance in the early stages of water deficit. Often, water stress in drip-irrigated orchard appears slowly, because of the high-frequency irrigation supply. Under this situation, the plants might develop mitigation strategies and adapt to water stress so that the stress does not affect significantly the crop, as happens in some cases under sustained deficit irrigation (Fereres and Soriano 2007). Therefore, in practical terms, sudden and moderate stress is the best strategy to identify those areas that are more sensitive to water stress within drip-irrigated agricultural fields.

The TSI accounts for static and dynamic variables; therefore, the maps were not identical from year to year. Some parts were identified as sensitive or resistant systematically, because of the static factors affecting the water status. Those areas affected by the dynamic factors varied from year to year. Multiple acquisitions over the same area can provide this type of information. Nevertheless, more research is needed to fine-tune the methodology and validate this hypothesis.

The optimal number of sensors to be deployed in the field will depend on the variability of the water status, which may be associated with the irrigation system, or crop or soil properties. Currently, the use of sensors to be deployed in the field to monitor water status is gaining interest even under commercial situations. Novel concepts, related to the IoT and sensors networks, are seeking to be implemented in the field. The optimal location for these will depend on the number of sensors available. When many sensors are available, they can be distributed in a grid pattern. Nevertheless, when only a few sensors are available, it is important to target the most representative areas. Bazzi et al. (2019) developed a methodology that identifies the best locations of point sensors according to the number of sensors available, and the variability of water status within tree and vine orchards, based on water potential and soil measurements. Remote identification of the variability within irrigated fields and the zoning according to the response to water stress may provide valuable information to determine what is the optimal number of sensors to be deployed and where these sensors should be installed. Analysis of the histogram of TSI at the beginning of the season allows the identification of homogeneous zones, according to the sensitivity to water stress. Moreover, if the study is repeated during the season, the information can be updated accordingly. In this work, the areas that are more prone to water stress have been systematically identified. By targeting these areas with point sensors, it is possible to detect water stress in the early stages and recalculate the irrigation accordingly. This procedure might be of special interest in those years when water is available. When water is scarce, or when the economic value of the crop yield is expected to be low, sensors can be deployed in areas displaying an “average behavior”.

The concept of precision irrigation involves the accurate assessment of water status and the precise application of this volume at the required time (Smith et al. 2010). Therefore, it implies a system that can adapt to the prevailing conditions. It can be based on the irrigation according to homogeneous sub-areas within the orchard (management zones), the site-specific application of water according to local needs or the remote (and real-time) information to be applied for irrigation scheduling. Initial developments of precision irrigation were focused on site-specific irrigation systems, based on the modification of center pivot and lateral move irrigation machines to give spatially varied applications of water and nitrogen (Evans et al. 1996; Sadler et al. 1996). The potential water savings (under non-stressed conditions) of these site-specific irrigation systems may be in the range of 10 to 15% (Sadler et al. 2005), although more research is required to quantify water savings by a variable-rate application.

Tree nutrient status and the overall field management can affect the response of the crop to water application. It is well known that nitrogen deficiency may affect water relations (Radin and Parker 1979; Jacob et al. 1995). This could be in relation with fertilization management, but also any other application or operation that are carried out in the field determining the overall crop performance. This can be even more important in the case of peach orchards, which are intensively managed farming systems where operations such as fruit thinning, summer pruning, among others are intensively performed. These effects were not considered in this study, and might also influence the scatter of the data and be responsible for part of the apparent discrepancies observed among years. Further research might focus some of these effects, by, for example, including some indicators related to nitrogen content and chlorophyll fluorescence as a proxy for plant photosynthesis.

Conclusion

A new indicator called Thermal Sensitivity Index (TSI) was developed using the high-resolution thermal imagery obtained at two dates, before and after moderate water tress was applied in commercial peach orchards. The index accounts for the rate of change in water status between the two dates. It also incorporates information about the climatic conditions during the stress period, using the cumulated thermal time. The index was demonstrated to be related to the rate of change of stem water potential between the two dates ($R^2 = 0.57$). This approach allows the identification of water-stress sensitive areas in the orchards. The maps showed some spatial consistency among years. Future work should verify other sources of variability affecting the index, particularly related to nutrient status and farm management practices.

Acknowledgements Authors acknowledge Rafa Romero, Alberto Vera and David Notario for their technical support with imagery acquisition and processing; and José S. Rubio-Asensio, Margarita Parra, Ignacio Buesa, Alejandro Martínez, Antonio Yeves, Felipe Sanz, David Hortelano and Diego Guerra for their help with field measurements.

Funding This research was funded in the frame of the collaborative international consortium IRIDA financed under the ERA-NET Cofund Water-Works 2014 Call with Spanish national funds from the Agencia Estatal de Investigación grant PCIN-2015-263. This ERA-NET is an integral part of the 2015 Joint Activities developed by the Water Challenges for a Changing World Joint Programme Initiative (Water JPI) JPIWaterWaterWorks 2014. Funding from the Spanish Ministry of Science and Innovation (AGL2017-90666-REDC and RTI2018-096754-J-I00) is also acknowledged. V.G.-D. was supported by a postdoctoral scholarship from the 'Ramon y Cajal' programme Spanish Ministry of Economy and Competitiveness (RYC2018-024994-I).

References

Agam, N., Cohen, Y., Alchanatis, V., & Ben-Gal, A. (2013). How sensitive is the CWSI to changes in solar radiation? *International Journal of Remote Sensing, 34*, 6109–6120.

Bazzi, C. L., Schenatto, K., Upadhyaya, S., Rojo, F., Kizer, E., & Ko-Madden, C. (2019). Optimal placement of proximal sensors for precision irrigation in tree crops. *Precision Agriculture, 20*(4), 663–674.

Bellvert, J., Zarco-Tejada, P. J., Marsal, J., Girona, J., Gonzalez-Dugo, V., & Fereres, E. (2016). Vineyard irrigation scheduling based on airborne thermal imagery and water potential thresholds. *Australian Journal of Grape and Wine Research, 22*(2), 307–315.

Ben-Gal, A., Agam, N., Alchanatis, V., Cohen, Y., Yermiyahu, U., Zipori, I., et al. (2009). Evaluating water stress in irrigated olives: Correlation of soil water status, tree water status, and thermal imagery. *Irrigation Science, 27*(5), 367–376.

Berni, J. A. J., Zarco-Tejada, P. J., Gonzalez-Dugo, V., & Fereres, E. (2009). Remote sensing of thermal water stress indicators in peach. *Acta Horticulturae, 962*, 325–331.

Camp, C. R., & Sadler, E. J. (1998). Site-specific crop management with a center pivot. *Journal of Soil and Water Conservation, 53*(4), 312–314.

Cohen, Y., Alchanatis, V., Saranga, Y., Rosenberg, O., Sela, E., & Bosak, A. (2017). Mapping water status based on aerial thermal imagery: comparison of methodologies for upscaling from a single leaf to commercial fields. *Precision Agriculture, 18*(5), 801–822.

Conesa, M. R., Conejero, W., Vera, J., Ramírez-Cuesta, J. M., & Ruiz-Sánchez, M. C. (2019). Terrestrial and Remote Indexes to Assess Moderate Deficit Irrigation in Early-Maturing Nectarine Trees. *Agronomy, 9*(10), 630.

Dag, A., Cohen, Y., Alchanatis, V., Zipori, I., Sprinstin, M., Cohen, A., et al. (2015). Automated detection of malfunctions in drip-irrigated systems using thermal remote sensing in vineyards and olive orchards. In J. V. Stafford (Ed.), *Proceedings of the 10th European Conference on Precision Agriculture* (pp 519–525). Wageningen, The Netherlands: Wageningen Academic Publisher.

Dukes, M. D., & Perry, C. (2006). Uniformity testing of variable-rate center pivot irrigation control systems. *Precision Agriculture, 7*(3), 205–218.

Evans, R. G., Han, S., Schneider, S. M., & Kroeger, M. W. (1996). Precision center pivot irrigation for efficient use of water and nitrogen. In P. C. Robert, R. H. Rust, W. E. Larson (Eds.), *Proceedings of the 3rd International Conference on Precision Agriculture*. Madison, WI: ASA, CSSA, SSSA.

Fereres, E., Goldhamer, D. A., & Parsons, L. R. (2003). Irrigation water management of horticultural crops. *Hortscience, 38*(5), 1036–1042.

Fereres, E., & Soriano, M. A. (2007). Deficit irrigation for reducing agricultural water use. *Journal of Experimental Botany, 58*(2), 147–159.

Gilabert, M. A., Gandía, S., & Melia, J. (1996). Analyses of spectral-biophysical relationships for a corn canopy. *Remote Sensing of Environment, 55*(1), 11–20.

Girona, J., & Fereres, E. (2012). Peach. In P. Steduto, T. C. Hsiao, E. Fereres & D. Raes (Eds.), *Crop yield response to water* (pp. 392–406). Rome: FAO.

Gonzalez-Dugo, V., Goldhamer, D., Zarco-Tejada, P. J., & Fereres, E. (2015). Improving the precision of irrigation in a pistachio farm using an unmanned airborne thermal system. *Irrigation Science, 33*(1), 43–52.

Gonzalez-Dugo, V., Lopez-Lopez, M., Espadafor, M., Orgaz, F., Testi, L., Zarco-Tejada, P. J., Lorite, I. J., & Fereres, E. (2019). Transpiration from canopy temperature: Implications for the assessment of crop yield in almond orchards. *European Journal of Agronomy, 105*, 78–85.

Gonzalez-Dugo, V., Zarco-Tejada, P. J., & Fereres, E. (2014). Applicability and limitations of using the crop water stress index as an indicator of water deficits in citrus orchards. *Agricultural and Forest Meteorology, 198,* 94–104.

Hsiao, T. C., Fereres, E., Acevedo, E., & Henderson, D. W. (1976). Water stress and dynamics of growth and yield of crop plants. In *Water and plant life* (Vol. 19). Ecological studies. Berlin: Springer.

Idso, S. B., Jackson, R. D., Pinter, P. J. J., Reginato, R. J., & Hatfield, J. L. (1981). Normalizing the stress-degree-day parameter for environmental variability. *Agricultural Meteorology, 24,* 45–55.

Jacob, J., Udayakumar, M., & Prasad, T. G. (1995). Mesophyll conductance was inhibited more than stomatal conductance in nitrogen deficient plants. *Plant Physiology and Biochemistry, 17*, 55–61.

Johnson, R. S., Handley, D. F., & DeJong, T. M. (1992). Long-term response of early maturing peach trees to postharvest water deficits. *Journal of the American Society for Horticultural Science, 117*, 881–886.

Jones, H. G., Stoll, M., Santos, T., Sousa, C. D., Chaves, M. M., & Grant, O. M. (2002). Use of infrared thermography for monitoring stomatal closure in the field: Application to grapevine. *Journal of Experimental Botany, 53*(378), 2249–2260.

McClymont, L., Goodwin, I., Mazza, M., Baker, N., Lanyon, D. M., Zerihun, A., et al. (2012). Effect of site-specific irrigation management on grapevine yield and fruit quality attributes. *Irrigation Science, 30*, 461–470.

O'Shaughnessy, S. A., Evett, S. R., & Colaizzi, P. D. (2015). Dynamic prescription maps for site-specific variable rate irrigation of cotton. *Agricultural Water Management, 159*, 123–138.

Radin, J. W., & Parker, L. L. (1979). Water relations of cotton plants under nitrogen deficiency. II. Environmental interactions on stomata. *Plant Physiology, 64,* 499–501.

Ramírez-Cuesta, J. M., Kilic, A., Allen, R., Santos, C., & Lorite, I. J. (2017). Evaluating the impact of adjusting surface temperature derived from landsat 7 ETM+ in crop evapotranspiration assessment using high-resolution airborne data. *International Journal of Remote Sensing, 38*(14), 4177–4205.

Sadler, E. J., Camp, C. R., Evans, D. E., & Usrey, L. J. (1996). A site-specific center pivot irrigation system for highly variable coastal plain soils. In P. C. Robert, R. H. Rust, W. E. Larson (Eds.), *Proceedings of the 3rd International Conference on Precision Agriculture*. Madison, WI: ASA, CSSA, SSSA.

Sadler, E. J., Evans, R. G., Stone, K. C., & Camp, C. R. (2005). Opportunities for conservation with precision irrigation. *Journal of Soil and Water Conservation, 60*(6), 371–379.

Schepers, A. R., Shanahan, J. F., Liebig, M. A., Schepers, J. S., Johnson, S. H., & Luchiari, A. Jr. (2004). Appropriateness of Management Zones for Characterizing Spatial Variability of Soil Properties and Irrigated Corn Yields across Years. *Agronomy Journal, 96*(1), 195–203.

Smith, R. J., Baillie, J. N., McCarthy, A. C., Raine, S. R., & Baillie, C. P. (2010). Review of precision irrigation technologies and their application. Project Report. Toowoomba: University of Southern Queensland, National Centre for Engineering in Agriculture.

Testi, L., Goldhamer, D. A., Iniesta, F., & Salinas, M. (2008). Crop water stress index is a sensitive water stress indicator in pistachio trees. *Irrigation Science, 26*, 395–405.

Yan, L., Zhou, S., Cifang, W., Hongyi, L., & Feng, L. (2007). Classification of management zones for precision farming in saline soil based on multi-data sources to characterize spatial variability of soil properties. *Transactions of the Chinese Society of Agricultural Engineering, 23*(8), 84–89.

Zarco-Tejada, P. J., Gonzalez-Dugo, V., & Berni, J. A. J. (2012). Fluorescence, temperature and narrow-band indices acquired from a UAV platform for water stress detection using a micro-hyperspectral imager and a thermal camera. *Remote Sensing of Environment, 117*, 322–337.